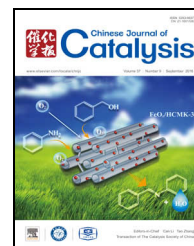


available at [www.sciencedirect.com](http://www.sciencedirect.com)journal homepage: [www.elsevier.com/locate/chnjc](http://www.elsevier.com/locate/chnjc)

## Article

# Aerobic oxidative coupling of alcohols and amines to imines over iron catalysts supported on mesoporous carbon



Longlong Geng, Jinling Song, Bin Zheng, Shujie Wu, Wenxiang Zhang, Mingjun Jia, Gang Liu\*

Key Laboratory of Surface and Interface Chemistry of Jilin Province, College of Chemistry, Jilin University, Changchun 130012, Jilin, China

## ARTICLE INFO

## Article history:

Received 30 May 2016

Accepted 12 July 2016

Published 5 September 2016

## Keywords:

Iron catalyst

Imine synthesis

Oxidative coupling

Mesoporous carbon

Molecular oxygen

## ABSTRACT

Direct oxidative coupling of an alcohol and amine, with air or molecular oxygen as the oxygen source, is an environmentally friendly method for imine synthesis. We developed an Fe catalyst supported on mesoporous carbon (denoted by FeO<sub>x</sub>/HCMK-3) for this reaction with excellent activity and recyclability. FeO<sub>x</sub>/HCMK-3 was prepared by impregnating HNO<sub>3</sub>-treated mesoporous carbon (CMK-3) with iron nitrate solution. The highly dispersed FeO<sub>x</sub> species give FeO<sub>x</sub>/HCMK-3 high reducibility and are responsible for the high catalytic performance. Imine synthesis over FeO<sub>x</sub>/HCMK-3 follows a redox mechanism. The oxygen species in FeO<sub>x</sub>/HCMK-3 participate in the reaction and are then regenerated by oxidation with molecular O<sub>2</sub>. The reaction involves two consecutive steps: oxidative dehydrogenation of an alcohol to an aldehyde and coupling of the aldehyde with an amine to give an imine. Oxidative dehydrogenation of the alcohol is the rate-determining step in the reaction.

© 2016, Dalian Institute of Chemical Physics, Chinese Academy of Sciences.  
Published by Elsevier B.V. All rights reserved.

## 1. Introduction

Imines are important nitrogen compounds; they contain a reactive C=N moiety [1,2]. Imines are nitrogen sources and can undergo various transformations. They are widely used in biological, agricultural, and pharmaceutical synthetic processes [3–6]. The condensation of aldehydes or ketones with amines is the traditional method for imine synthesis, and is usually performed in the presence of an acidic catalyst [7–9]. Recently, the direct oxidative coupling of an alcohol and amine to give an imine has attracted increasing attention because of its environmentally friendly properties [10–16]. Air or molecular oxygen can be used as the oxygen source for the production of various types of desirable imines from appropriate alcohols and amines as starting reagents, with water as the only by-product. Effective noble-metal-based homogeneous and

heterogeneous catalysts such as supported Au, Ru, Pd, and Pt have been reported [17–24]. However, the high price of these noble metals and the need to use inorganic or organic bases as additives in the reaction system limit their large-scale application in imine synthesis.

Recently, a few metal oxide catalysts that can catalyze this imine synthesis have been reported [25–27]; for example, CeO<sub>2</sub> is an effective catalyst for imine formation from benzyl alcohol and aniline at low temperature (60 °C), with a high yield of 96% after 24 h [25]. Manganese oxides supported on hydroxyapatite (MnO<sub>x</sub>/HAP) also show high activity in the oxidative coupling of alcohols and amines [26]. When benzyl alcohol and aniline were used, a 92% yield of the imine was obtained after reaction for 24 h at 80 °C. The catalytic activity, especially the capacity to activate molecular oxygen, is highly dependent on the redox properties of the metal oxides. They determine the

\* Corresponding author. Tel: +86-431-85155390; Fax: +86-431-88499140; E-mail: [lgang@jlu.edu.cn](mailto:lgang@jlu.edu.cn)

This work was supported by the National Natural Science Foundation of China (21473073, 21473074) and the "13th Five-Year" Science and Technology Research of the Education Department of Jilin Province (2016403).

DOI: 10.1016/S1872-2067(16)62506-8 | <http://www.sciencedirect.com/science/journal/18722067> | Chin. J. Catal., Vol. 37, No. 9, September 2016

catalytic behavior of the metal oxide in the oxidative dehydrogenation step. Tuning the redox properties of metal oxide catalysts should therefore be an efficient method for developing high-performance catalysts for imine synthesis via oxidative coupling.

Among various metal oxides, iron oxides have the advantages of ready availability, low cost, and low toxicity [28–32]. However, iron oxides show low activities in the oxidative coupling of alcohols and amines to imines [25]. This could be related to the intrinsic inert properties of a bulk material, such as a low surface-to-bulk atomic ratio and low surface energy. We recently reported that the redox properties of iron oxides can be tuned by forming highly dispersed iron oxide species on carbon supports [33,34]. The catalysts show high redox activities in  $O_2$  activation. This property of these iron oxide species might enable them to catalyze oxidative coupling of alcohols and amines to imines.

In this work, carbon-supported  $FeO_x$  ( $FeO_x/HCMK-3$ ) was used as a catalyst for oxidative coupling of alcohols and amines to imines. A 98.8% yield of imine was obtained in the oxidative coupling of benzyl alcohol and aniline after reaction for 6 h at 80 °C. The  $FeO_x/HCMK-3$  catalyst was efficient in the synthesis of a series of imine compounds. The correlations between the activity and physicochemical properties of the catalyst were investigated based on a series of characterization results. The reaction mechanism of imine synthesis over  $FeO_x/HCMK-3$  was also explored.

## 2. Experimental

### 2.1. Materials

All chemicals were analytical grade and used without further purification. Double-distilled water was used in all experiments.

### 2.2. Catalyst preparation

SBA-15 templates were prepared using a triblock copolymer,  $EO_{20}-PO_{70}-EO_{20}$  (P123; EO: ethylene oxide; PO: propylene oxide), as the surfactant and tetraethyl orthosilicate (TEOS) as the silica source, using the procedure reported by Zhao et al. [35]. Typically, TEOS (4.68 mL) was added to 2 mol/L HCl (60 mL) containing P123 (2 g) at 35 °C. After stirring in a water bath (35 °C) for 24 h, the mixture was transferred to Teflon-lined stainless steel autoclaves (100 mL) and heated to 100 °C for 3 d. The resultant solid product was separated by filtration, dried at 100 °C for 12 h, and calcined at 550 °C for 6 h.

CMK-3 was prepared using SBA-15 as a hard template and sucrose as the carbon source [36]. Typically, SBA-15 silica (1.0 g) was added to a solution containing sucrose (1.25 g), sulfuric acid (0.14 g), and distilled water (5.0 g). The mixture was kept in an oven for 6 h at 80 °C. The temperature was then increased to 160 °C and maintained for 6 h. The heating procedure was repeated after addition of the carbon precursor (0.8 g of sucrose, 0.09 g of  $H_2SO_4$ , and 5.0 g of  $H_2O$ ) to achieve complete infiltration of the internal pores of the SBA-15 silica. The car-

bon-silica composite was obtained by pyrolysis at 900 °C for 6 h under an Ar flow and then washing in 10 wt% HF aqueous solution to remove the silica template.

The carbon-supported iron oxide catalyst was prepared using a wet impregnation method. Typically, an Fe-containing solution was obtained by dissolving  $Fe(NO_3)_3 \cdot 9H_2O$  in a certain amount of water. Before added to the iron nitrate solution, the CMK-3 support was treated in 4 mol/L  $HNO_3$  solution at 60 °C for 6 h (denoted by HCMK-3). After stirring for about 3 h at room temperature, the mixture was heated at 80 °C under atmospheric pressure to evaporate the water. The as-synthesized catalyst was thermally treated at 400 °C for 4 h under an Ar flow. The iron oxide loading was 5 wt% (calculated based on  $Fe_2O_3$ ) and the resultant material was denoted by  $FeO_x/HCMK-3$ . For comparison, a sample consisting of  $Fe^{3+}$  ions supported on HCMK-3 (denoted by Fe-HCMK-3) was also prepared by the same impregnation method and using  $HNO_3$ -treated CMK-3 as a support. The difference was that after impregnation the sample was dried in an oven at 80 °C for 12 h without further thermal treatment at 400 °C in an Ar flow for 4 h. The Fe species loading was the same as that on  $FeO_x/HCMK-3$ . Bulk  $Fe_2O_3$  was also prepared using a conventional precipitation method with  $Fe(NO_3)_3 \cdot 9H_2O$  as the Fe source and ammonia as the precipitating agent (pH 9). The resultant material was calcined at 400 °C for 4 h in air.

### 2.3. Catalyst characterization

Powder X-ray diffraction (XRD) patterns were recorded with a Rigaku X-ray diffractometer using  $Cu K\alpha$  radiation ( $\lambda = 1.5418 \text{ \AA}$ ). Transmission electron microscopy (TEM) images and high-angle annular dark field scanning TEM (HAADF-STEM) images were obtained using a FEI Tecnai F20 instrument with an accelerating voltage of 200 kV, equipped with an energy-dispersive X-ray spectroscopy analyzer. X-ray photoelectron spectroscopy (XPS) was performed using a Thermo ESCA LAB 250 system with an  $Mg K\alpha$  source (1254.6 eV).  $N_2$  adsorption-desorption isotherms were recorded at  $-196 \text{ °C}$  using a Micromeritics ASAP 2010N analyzer. Raman spectra were recorded using a Bruker RFS 100 Raman spectrometer with an Ar laser (532 nm) as the excitation source. Temperature-programmed reduction (TPR) was performed using a Tianjin Xianquan TP-5079 adsorption analyzer. Before examination, the catalysts (30 mg of  $FeO_x/HCMK-3$ , 10 mg of  $Fe_2O_3$ ) were treated in an Ar (99.99%) flow at 400 °C for 30 min. The zeta-potential curve was plotted as a function of pH, from 2 to 8 (Zeta PALS analyzer, Brookhaven Instruments Corporation, USA). The sample was suspended in aqueous 0.01 mol/L NaCl solution. The pH was adjusted using 1.0 mol/L NaOH and HCl solutions. The Fe content was estimated using inductively coupled plasma atomic emission spectroscopy (ICP-AES; Perkin-Elmer emission spectrometer). Fourier transform infrared (FT-IR) spectra were recorded using a Thermo Nicolet 6700 FT-IR spectrometer. The Boehm titration method was used to determine the amounts of surface groups. The carbon support (100 mg) was placed in 10 mL of a 0.05 mol/L solution containing NaOH,  $Na_2CO_3$ , and  $NaHCO_3$ . The

vials were sealed and shaken for 24 h, and the contents were filtered. A known quantity of HCl was added to each filtrate. The excess acid left in the solution was titrated with NaOH using an automatic potentiometer titrator (LeiCi ZDT-4A). The amounts of acidic sites were calculated based on the assumption that NaOH neutralizes carboxylic, phenolic, and lactonic groups, NaHCO<sub>3</sub> neutralizes carboxylic groups, and Na<sub>2</sub>CO<sub>3</sub> neutralizes carboxylic and lactonic groups.

#### 2.4. Catalytic tests

The aerobic oxidative coupling of an alcohol and amine was performed in a 50-mL two-necked flask at atmospheric pressure. A quantity of catalyst (0.3 g) was added to the reactor containing alcohol (1.0 mmol), amine (2.0 mmol), and toluene (10 mL). The mixture was in contact with air, and the reaction temperature was kept at 80 °C. The reaction mixture was extracted via a sampling pipe with a filtrator and then transferred to a vial. The products were analyzed using a gas chromatograph equipped with an HP-5 column and a flame ionization detector. The conversion and yield of the imine product were calculated based on the alcohol to imine ratio. The products were identified using standard compounds and gas chromatography-mass spectrometry. The turnover frequencies (TOFs) were calculated based on benzyl alcohol conversion in the initial stage (60 min) and the amount of FeO<sub>x</sub> in the catalyst.

An oxygen-free experiment was performed in a Schlenk tube. First, the FeO<sub>x</sub>/HCMK-3 catalyst was put in a Schlenk tube, and degassed at 80 °C for 1.5 h under vacuum to remove adsorbed O<sub>2</sub>. High-purity N<sub>2</sub> (99.99%) was injected into the Schlenk tube until the pressure was 1 atm. The degassed toluene, benzyl alcohol, and aniline were added to the Schlenk tube. The system was further degassed and balanced with high purity N<sub>2</sub>. The Schlenk tube was then put in an oil bath (80 °C) to start the reaction. After each sample extraction, the system was degassed and balanced with high purity N<sub>2</sub>. All these treatments were to ensure the removal of molecular O<sub>2</sub> from the system. In the recycling experiments, the solid catalyst was separated by filtration and treated at 400 °C for 1 h before the next cycle.

### 3. Results and discussion

#### 3.1. Catalyst structure and surface properties

Fig. 1 shows the preparation of the carbon-supported FeO<sub>x</sub> (5 wt%, calculated based on Fe<sub>2</sub>O<sub>3</sub>) catalyst. The catalyst support was ordered mesoporous carbon CMK-3 prepared via a hard-template method. The CMK-3 was treated with 4 mol/L HNO<sub>3</sub> at 60 °C for 6 h before use as the catalyst support. The resultant carbon was denoted by HCMK-3. This was a key step in preparing a catalyst with highly dispersed FeO<sub>x</sub> species. A large amount of oxygen-containing functional groups formed on the HCMK-3 surface. Table 1 shows that the amounts of functional groups on HCMK-3, including carboxylic, lactonic, and phenolic groups, were all higher than those on CMK-3. The total amount of functional groups was about 1.47 mmol/g. The

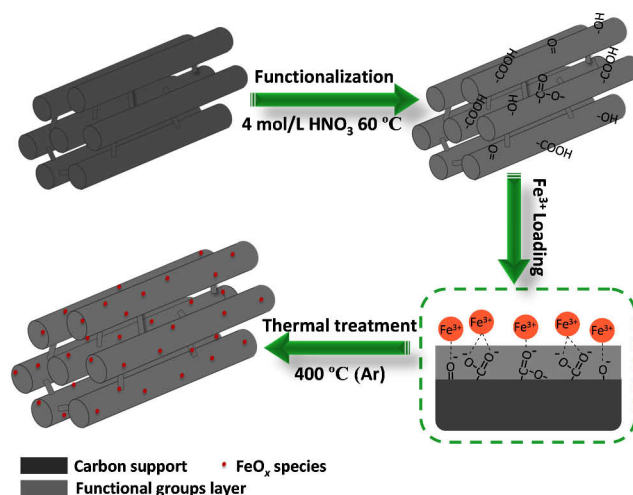


Fig. 1. Schematic illustration of synthetic route for FeO<sub>x</sub>/HCMK-3 preparation.

abundant functional groups endow the HCMK-3 support with a hydrophilic surface. This facilitates introduction of iron nitrate solution into the mesopores of the carbon support. The dried solid was calcined at 400 °C for 4 h in an Ar flow to give the FeO<sub>x</sub>/HCMK-3 catalyst.

The XRD patterns show that FeO<sub>x</sub>/HCMK-3 retains the ordered arrangement of the parent HCMK-3 support (Fig. 2a). The three diffraction peaks in the range  $2\theta = 0.75^\circ\text{--}3^\circ$  can be indexed to the (100), (110), and (200) reflections of the HCMK-3 hexagonal space group. Wide-angle XRD patterns show that both samples have two broad diffraction peaks, centered at 24.5° and 44° (Fig. 2b), which are assigned to diffractions from the (002) and (100) graphite planes of the carbon supports [37]. No crystalline phase related to iron oxides was observed, indicating that the iron oxide particles are small or the degree of crystallization is low. The Raman spectra of FeO<sub>x</sub>/HCMK-3 and HCMK-3 show two peaks, at 1358 and 1598 cm<sup>-1</sup>, which are assigned to the D and G bands of the carbon support (Fig. 2c) [38,39]. No peak below 1000 cm<sup>-1</sup> attributable to crystalline iron oxides can be observed [40,41]; this also indicates that the iron oxide particles in FeO<sub>x</sub>/HCMK-3 are small. The N<sub>2</sub> adsorption-desorption isotherms show that FeO<sub>x</sub>/HCMK-3 gives isotherms typical of an ordered mesostructure (type IV) with a well-defined step in the adsorption curve near  $p/p_0 = 0.5$  (Fig. 2d). The surface area, pore volume, and pore size of FeO<sub>x</sub>/HCMK-3 are similar to those of HCMK-3, indicating that the iron oxides do not block the mesopores of the CMK-3 support.

TEM images confirm that FeO<sub>x</sub>/HCMK-3 retains the ordered structure of the CMK-3 support (Fig. 3a). No Fe particles were observed in the region examined, even at high resolution (Fig.

Table 1

Boehm titration results for CMK-3 and HCMK-3.

Sample	Content of functional groups (mmol/g)			
	Carboxylic	Lactonic	Phenolic	Acidic
CMK-3	0.01	0.11	0.12	0.24
HCMK-3	0.24	0.34	0.89	1.47

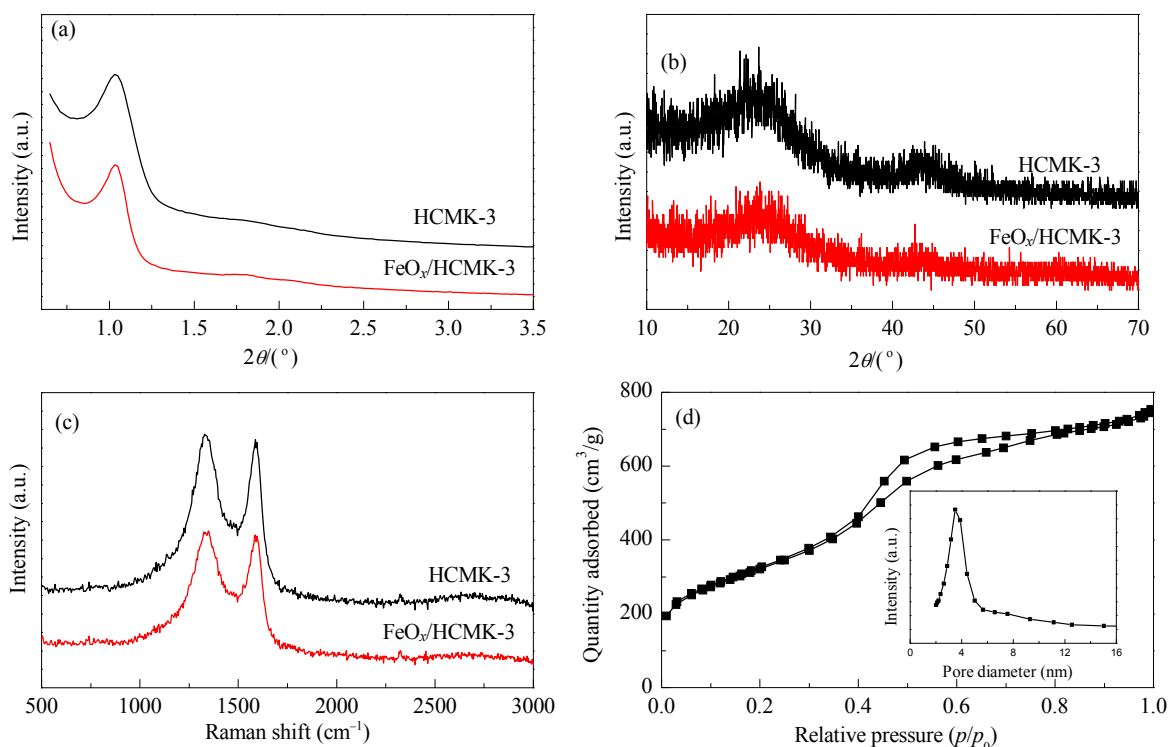


Fig. 2. Low-angle (a) and wide-angle (b) XRD patterns for HCMK-3 and  $\text{FeO}_x/\text{HCMK-3}$ ; (c) Raman spectra of HCMK-3 and  $\text{FeO}_x/\text{HCMK-3}$ ; (d)  $\text{N}_2$  adsorption-desorption isotherms of  $\text{FeO}_x/\text{HCMK-3}$  (inset shows pore size distribution).

3b and c). STEM and energy-dispersive X-ray mapping were performed to investigate iron oxide dispersion (Fig. 3d and e). The results show that Fe species are nearly homogeneously dispersed on the HCMK-3 surface, but the particle size still cannot be ascertained based on these measurements. A sample with a low  $\text{FeO}_x$  loading (0.25 wt%) was prepared to clarify the  $\text{FeO}_x$  dispersed state on the HCMK-3 surface.  $\text{FeO}_x$  particles still cannot be observed in the HRTEM image (not shown), but some light spots (about 2–3 nm) can be distinguished in the HAADF-STEM image (Fig. 3f). These results suggest that  $\text{FeO}_x$  species are present as two-dimensional or even sub-nano clusters. These clusters could be the constituent units of the highly dispersed  $\text{FeO}_x$  on the carbon support. The HRTEM and HAADF-STEM images together confirm that the  $\text{FeO}_x$  species are highly dispersed on the HCMK-3 support surface.

XPS shows that there are no obvious differences between the Fe 2p binding energies of  $\text{FeO}_x/\text{HCMK-3}$  and bulk  $\text{Fe}_2\text{O}_3$  (Fig. 4a). The Fe 2p<sub>1/2</sub> and Fe 2p<sub>3/2</sub> peaks appear at 724.2 and 710.9 eV, respectively. This indicates that most of the Fe species are present in the iron oxides in the +3 valence state [42,43]. Clear differences can be observed in the O 1s spectra. The binding energies in the deconvoluted O 1s XPS spectrum are in accordance with those reported in the literature [44,45]. The O 1s spectrum of bulk  $\text{Fe}_2\text{O}_3$  can be deconvoluted into two peaks (Fig. 4b). Peak I, in the range 529.5–530.5 eV, is assigned to O<sup>2-</sup> ions in the iron oxide lattice. Peak II, centered at about 532 eV, is related to oxygen in surface OH groups or oxygen vacancies in  $\text{Fe}_2\text{O}_3$ . The peak II/peak I area ratio is 0.21 for bulk  $\text{Fe}_2\text{O}_3$ . The  $\text{FeO}_x/\text{HCMK-3}$  O 1s spectrum can be deconvoluted into three peaks. The new peak (peak III) at 534 eV is attrib-

uted to oxygen functional groups remaining on the catalyst surface. The peak II/peak I area ratio is 3.54 for  $\text{FeO}_x/\text{HCMK-3}$ , which is much higher than that for bulk  $\text{Fe}_2\text{O}_3$ . This is caused by the small size of the iron oxide particles and interactions between iron oxides and the carbon support.

Diffuse reflectance infrared Fourier transform (DRIFT) spectra show that some oxygen-containing groups remain on the  $\text{FeO}_x/\text{HCMK-3}$  surface (Fig. 5a). Further FT-IR spectra were obtained to clarify whether the Fe species were located in iron oxides or present as  $\text{Fe}^{3+}$  ions coordinated with these functional groups. A sample consisting of  $\text{Fe}^{3+}$  ions supported on HCMK-3 (denoted by Fe-HCMK-3) was prepared via the same impregnation method as was used to prepare  $\text{FeO}_x/\text{HCMK-3}$ , with  $\text{HNO}_3$ -treated CMK-3 as a support. The Fe species loading was the same as that for  $\text{FeO}_x/\text{HCMK-3}$ . The difference is that after impregnation, the sample was dried in an oven at 80 °C for 12 h to obtain Fe-HCMK-3, whereas further thermal treatment at 400 °C in an Ar flow for 4 h is needed to obtain  $\text{FeO}_x/\text{HCMK-3}$ . The peak at 469  $\text{cm}^{-1}$  in the FT-IR spectrum of  $\text{FeO}_x/\text{HCMK-3}$  (Fig. 5b) can be attributed to the stretching vibration of Fe–O, similar to that of  $\text{Fe}_2\text{O}_3$ . However, this signal is different in the Fe-HCMK-3 spectrum. A combination of the FT-IR and XPS results confirms that Fe is mainly located in iron oxide species (i.e.,  $\text{FeO}_x$ ). The formation of  $\text{FeO}_x$  species in  $\text{FeO}_x/\text{HCMK-3}$  is a result of the high treatment temperature. The oxygen-containing functional groups in HCMK-3 can interact with these two-dimensional  $\text{FeO}_x$  species.

The  $\text{H}_2$ -TPR profiles (Fig. 6) show that the iron oxide species in  $\text{FeO}_x/\text{HCMK-3}$  are more reducible than those in bulk  $\text{Fe}_2\text{O}_3$ . There are three reduction peaks present in the profile of bulk

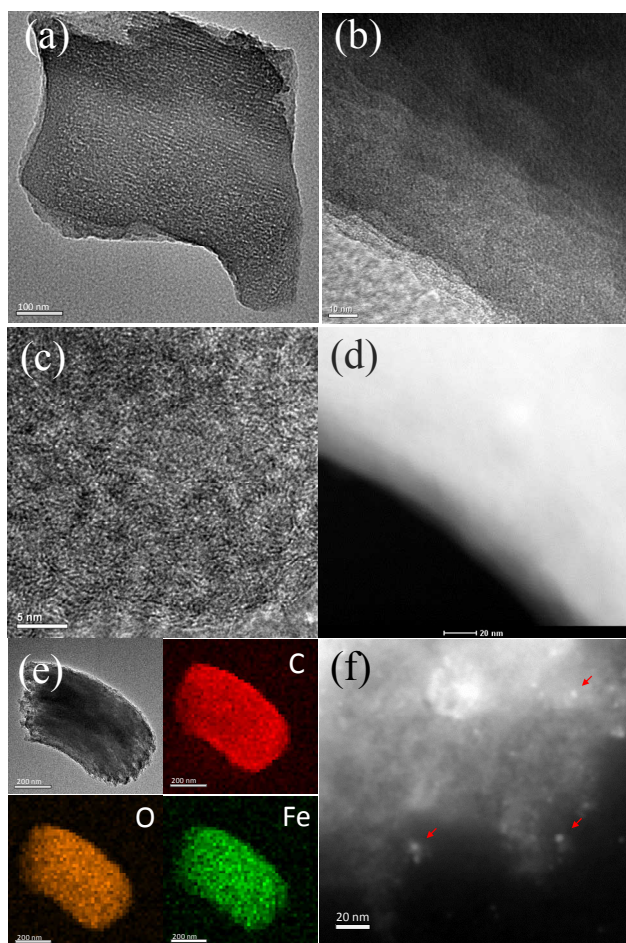


**Fig. 3.** TEM (a), HRTEM (b, c), HAADF-STEM (d), and energy-dispersive X-ray mapping images (e) of  $\text{FeO}_x/\text{HCMK-3}$ ; (f) HAADF-STEM image of 0.25wt%  $\text{FeO}_x/\text{HCMK-3}$  catalyst.

$\text{Fe}_2\text{O}_3$ . The narrow peak (centered at 430 °C) can be ascribed to the reduction of  $\text{Fe}_2\text{O}_3$  to  $\text{Fe}_3\text{O}_4$ . The two overlapping peaks in the range 450–800 °C can be ascribed to further reduction to  $\text{FeO}/\text{Fe}$  species [46,47]. For  $\text{FeO}_x/\text{HCMK-3}$ , only one broad peak is present in the range 200–600 °C. The start and center of this peak are clearly at lower temperatures than those for bulk  $\text{Fe}_2\text{O}_3$ , confirming the high reducibility of  $\text{FeO}_x/\text{HCMK-3}$ . The amounts of  $\text{H}_2$  consumed by  $\text{FeO}_x/\text{HCMK-3}$  and  $\text{Fe}_2\text{O}_3$  during

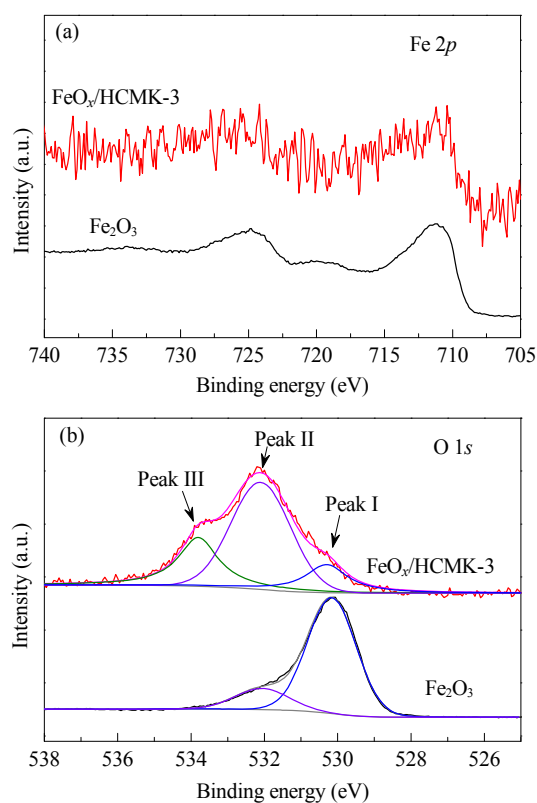


**Fig. 4.** Fe 2p (a) and O 1s (b) XPS spectra of  $\text{FeO}_x/\text{HCMK-3}$  and bulk  $\text{Fe}_2\text{O}_3$ .

TPR were 2.13 and 18.10 mmol/g, respectively. The  $\text{FeO}_x$  content in  $\text{FeO}_x/\text{HCMK-3}$  was 5 wt%, therefore the stoichiometric consumption of  $\text{H}_2$  by  $\text{FeO}_x$  should be 0.93 mmol/g, which is lower than the actual amount of  $\text{H}_2$  consumed (2.13 mmol/g). A combination of the  $\text{H}_2$ -TPR, XPS, and DRIFT results shows that additional  $\text{H}_2$  is consumed (1.2 mmol/g) because of the presence of oxygen-containing functional groups in  $\text{FeO}_x/\text{HCMK-3}$ . The quantity of reduced functional groups in  $\text{FeO}_x/\text{HCMK-3}$  was determined based on  $\text{H}_2$ -TPR of HCMK-3. The results show that  $\text{H}_2$  consumption by HCMK-3 was about 1.08 mmol/g, which is consistent with  $\text{H}_2$  consumption by the carbon support in  $\text{FeO}_x/\text{HCMK-3}$  (1.2 mmol/g).

These results show that oxygen functional groups play im-

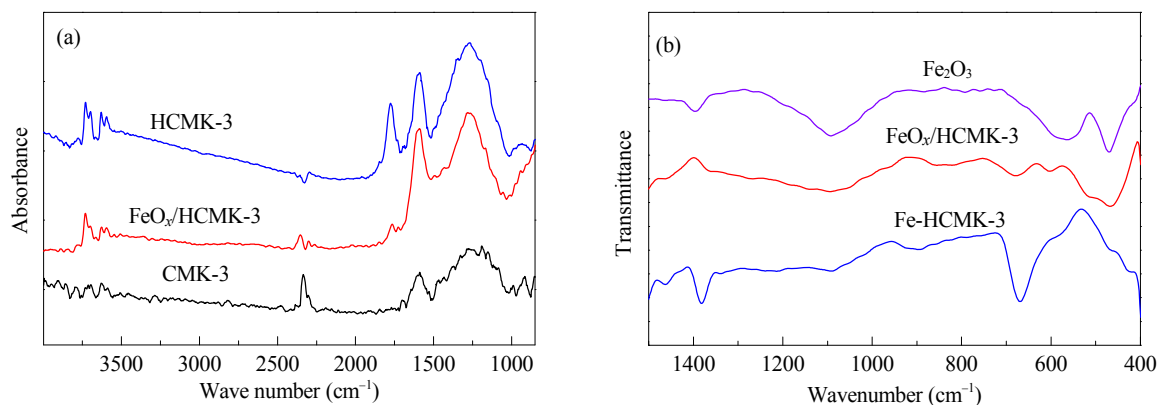


**Fig. 5.** (a) DRIFT spectra of CMK-3, HCMK-3, and  $\text{FeO}_x/\text{HCMK-3}$ ; (b) FT-IR spectra of  $\text{FeO}_x/\text{HCMK-3}$ , Fe-HCMK-3, and  $\text{Fe}_2\text{O}_3$ .

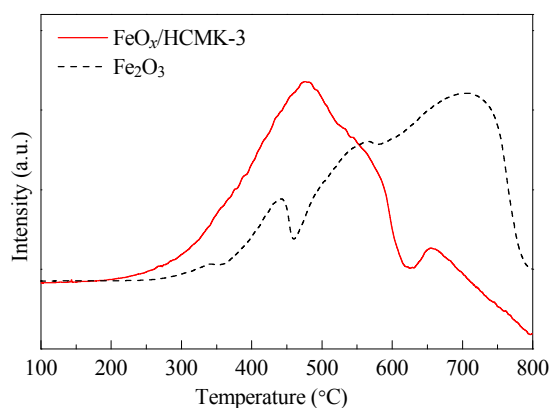


Fig. 6. H<sub>2</sub>-TPR profiles of FeO<sub>x</sub>/HCMK-3 and bulk Fe<sub>2</sub>O<sub>3</sub>.

portant roles in the formation of highly dispersed iron oxide species. They render the HCMK-3 support surface negatively charged. Zeta-potential measurements show that HCMK-3 is negatively charged at pH 1.0–8.0 (Fig. 7). Untreated CMK-3 is positively charged at pH less than 5.1. FeO<sub>x</sub>/HCMK-3 was prepared by impregnation with Fe(NO<sub>3</sub>)<sub>3</sub> aqueous solution. The pH of the Fe<sup>3+</sup>-containing solution was 1.65 (Fig. 7). Under these preparation conditions, there is an electrostatic force between the positively charged metal ions and negatively charged carbon surface (Fig. 1). This could be the main reason for the homogeneous dispersion of Fe ions on the carbon surface. In the subsequent thermal treatment, these surface oxygen functional groups provide strongly active sites for anchoring FeO<sub>x</sub> species, and suppress iron oxide aggregation.

### 3.2. Catalytic performance

Fig. 8 shows the catalytic activity of FeO<sub>x</sub>/HCMK-3 in the oxidative coupling of benzyl alcohol and aniline to an imine at 80 °C. The imine was identified using gas chromatography-mass spectrometry. For comparison, the reaction was also performed using bulk Fe<sub>2</sub>O<sub>3</sub> and HCMK-3. The activity of bulk Fe<sub>2</sub>O<sub>3</sub> was low. Only a 13.2% yield of imine was obtained after reaction for 8 h at 80 °C. The HCMK-3 support was almost inactive under the test conditions. For FeO<sub>x</sub>/HCMK-3, the yield

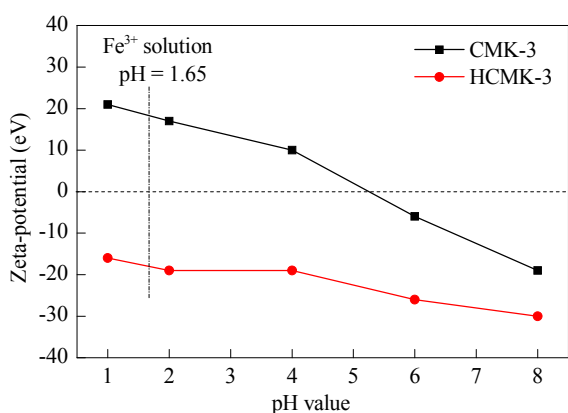


Fig. 7. Zeta-potential profiles for CMK-3 and HCMK-3; pH is the value for impregnation process, i.e., iron nitrate solution containing HCMK-3.

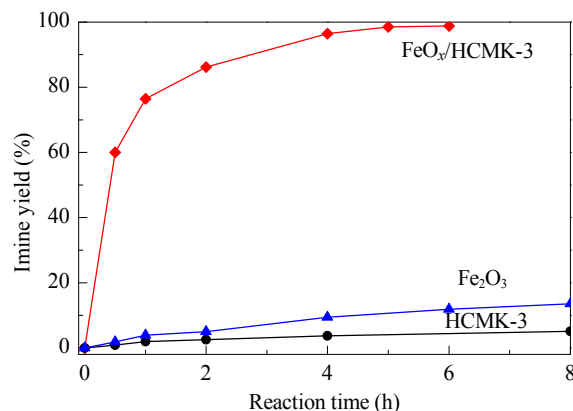


Fig. 8. Time dependences of imine formation from aerobic oxidative coupling of benzyl alcohol and aniline over FeO<sub>x</sub>/HCMK-3, bulk Fe<sub>2</sub>O<sub>3</sub>, and HCMK-3. Reaction conditions: benzyl alcohol 1 mmol, aniline 2 mmol, catalyst 0.3 g, toluene 10 mL, 80 °C, air 1 bar.

of imine after reaction for 6 h was 98.8%. The TOF for FeO<sub>x</sub>/HCMK-3 in the initial stage was 2.9 h<sup>-1</sup>. The catalytic performance of FeO<sub>x</sub>/HCMK-3 at 60 °C was also investigated for comparison with those of other reported catalytic systems. The TOF was 0.6 h<sup>-1</sup>. Comparisons with results reported in the literature [19,25,26] show that this TOF is higher than those for non-noble-metal oxide catalysts (e.g., CeO<sub>2</sub> and MnO<sub>x</sub>/HAP), but a little lower than those of supported Au catalysts under similar reaction conditions. The reaction was also performed using equimolar amounts of the alcohol and amine. A 78.4% yield of the imine was obtained after reaction for 8 h. All these results indicate that FeO<sub>x</sub>/HCMK-3 is an effective catalyst for imine formation.

Multiple aerobic oxidation cycles were performed to examine the recoverability of FeO<sub>x</sub>/HCMK-3 (Fig. 9). The catalyst retained high activity after five cycles, with only 3% and 5% decreases in the third and fifth cycles compared with the first one. Loss of Fe from the catalyst to the reaction mixture was determined using ICP-AES. Trace amounts of Fe (0.02 ppm, 0.02‰ of total Fe) were detected, indicating that Fe active sites

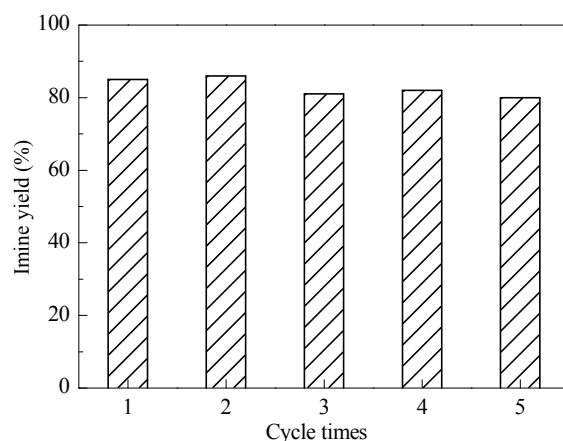


Fig. 9. Reusability of FeO<sub>x</sub>/HCMK-3 in imine synthesis by aerobic oxidative coupling of benzyl alcohol and aniline. Reaction conditions: benzyl alcohol 1 mmol, aniline 2 mmol, catalyst 0.3 g, toluene 10 mL, 80 °C, air 1 bar, 3 h. Recovered catalysts were treated under Ar at 400 °C for 1 h.

were not lost. The XRD patterns show that there was no aggregation of iron oxide species in the used FeO<sub>x</sub>/HCMK-3. All these results suggest that iron oxide active sites are stable in the FeO<sub>x</sub>/HCMK-3 catalyst. The decrease in the imine yield was mainly caused by loss of catalyst in the recycling process. The catalyst was recycled by filtration and then thermally treated at 400 °C for 1 h under Ar to remove adsorbed reagents. Catalyst loss (about 7%) is inevitable during this process.

Experiments were performed to identify the active sites in FeO<sub>x</sub>/HCMK-3 (Table 2). When Fe(NO<sub>3</sub>)<sub>3</sub> was used as the catalyst, the yield of imine after reaction for 8 h was 1.8%. Even in the co-presence of Fe(NO<sub>3</sub>)<sub>3</sub> and HCMK-3, the imine yield was only 5.0%. These results differ from those reported by Zhang et al. [48], mainly because different reaction conditions were used. Under their reaction conditions, Fe(NO<sub>3</sub>)<sub>3</sub> shows moderate activity in imine synthesis and the activity can be greatly enhanced by addition of 2,2,6,6-tetramethyl-1-piperidinyloxy [48]. We also investigated the catalytic performance of Fe-HCMK-3. An imine yield of 24.6% was obtained over Fe-HCMK-3 after reaction for 8 h; this is much lower than the yield achieved using FeO<sub>x</sub>/HCMK-3. Loss of Fe into the reaction mixture was detected using ICP-AES; the amount was about 33.65 ppm, which is 3.2% of the total amount of Fe loaded on Fe-HCMK-3. All these results suggest that Fe<sup>3+</sup> ions or coordinated Fe species were not active in the imine synthesis reaction. Supported FeO<sub>x</sub> species were the effective and stable active sites. The highly dispersed FeO<sub>x</sub> species on the HCMK-3 surface could affect the redox properties of the FeO<sub>x</sub>/HCMK-3 catalyst. The reducibility of these iron oxide species could be responsible for the high activity in this reaction.

The general applicability of the FeO<sub>x</sub>/HCMK-3 catalyst was also investigated. Eleven imines were obtained by oxidative coupling of amines with various alcohols. Table 3 (entries 1–7) shows that the FeO<sub>x</sub>/HCMK-3 catalyst is active in reactions using benzyl alcohol derivatives with either electron-rich or electron-poor substituents, especially 4-methylbenzyl alcohol, 4-methoxybenzyl alcohol, and 4-isopropylbenzyl alcohol (the imine yields were 93.2%, 90.7%, and 84.2%, respectively, after reaction for 8 h). FeO<sub>x</sub>/HCMK-3 also catalyzed the reaction of phenethyl alcohol and allylic alcohols (e.g., *trans*-2-hexenol) with aniline to give the corresponding imines when the reaction temperature and time were increased (Table 3, entries 8 and 9). Table 3 shows that FeO<sub>x</sub>/HCMK-3 is active in the aerobic oxidative coupling of aliphatic amines (e.g., cyclohexylamine

**Table 2**

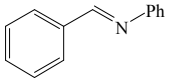
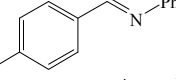
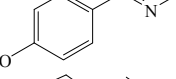
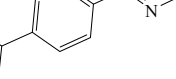
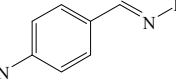
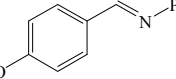
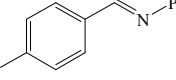
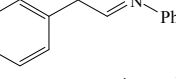
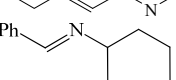
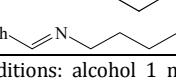
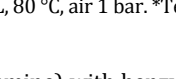
Imine synthesis by oxidative coupling of benzyl alcohol and aniline over various catalysts.

Entry	Catalyst	Time (h)	Yield (%)
1	FeO <sub>x</sub> /HCMK-3	6	98.6
2	None	8	0.9
3*	Fe(NO <sub>3</sub> ) <sub>3</sub>	8	1.8
4*	Fe(NO <sub>3</sub> ) <sub>3</sub> + HCMK-3	8	5.0
5	Fe-HCMK-3	8	24.6
6	Fe <sub>2</sub> O <sub>3</sub>	8	13.2
7	HCMK-3	8	5.1

Reaction conditions: benzyl alcohol 1 mmol, aniline 2 mmol, catalyst 0.3 g, toluene 10 mL, 80 °C, air 1 bar. \*The amount of Fe(NO<sub>3</sub>)<sub>3</sub> was calculated based on the Fe content in FeO<sub>x</sub>/HCMK-3.

**Table 3**

Aerobic oxidative coupling of various alcohols and anilines over FeO<sub>x</sub>/HCMK-3 catalyst.

$R^1-CH_2-CH_2-OH + R^2-NH_2 \xrightarrow[80\text{ }^\circ\text{C Air}]{\text{FeO}_x/\text{HCMK-3 catalyst}} R^1-CH=CH-R^2 + H_2O$			
Entry	Product	Time (h)	Yield (%)
1		6	98.0
2		8	93.2
3		8	90.7
4		8	84.2
5		8	80.7
6		10	75.1
7		10	64.2
8*		12	55.9
9*		12	36.4
10		8	85.8
11		8	80.6

Reaction conditions: alcohol 1 mmol, amine 2 mmol, catalyst 0.3 g, toluene 10 mL, 80 °C, air 1 bar. \*Temperature: 100 °C.

and *n*-butylamine) with benzyl alcohol (Table 3, entries 10 and 11). These results clearly show that FeO<sub>x</sub>/HCMK-3 is an efficient catalyst in oxidative coupling reactions.

Three additional experiments were performed to clarify the reaction mechanism over FeO<sub>x</sub>/HCMK-3; the results are shown in Fig. 10. Fig. 10a shows that the oxygen species in FeO<sub>x</sub>/HCMK-3 are active in the aerobic oxidative reaction. Even without the presence of O<sub>2</sub>, an 8.7% yield of imine was obtained after reaction for 8 h at 80 °C. This experiment was performed in a Schlenk tube (see the experimental section for details). The FeO<sub>x</sub>/HCMK-3 catalyst was first degassed at 80 °C for 1.5 h under vacuum to remove adsorbed O<sub>2</sub>. After adding the reactants and solvent, the system was further degassed and then balanced with high-purity N<sub>2</sub>. All these treatments were performed to ensure the removal of molecular O<sub>2</sub> from the system. This result shows that the oxygen species in FeO<sub>x</sub>/HCMK-3 participate in the reaction. The oxidative coupling of alcohols and amines on FeO<sub>x</sub>/HCMK-3 occur via a redox mechanism [25,26]. During imine synthesis over FeO<sub>x</sub>/HCMK-3, benzaldehyde was detected in the initial stage and the amount slowly decreased with time (Fig. 10b). This suggests that benzalde-

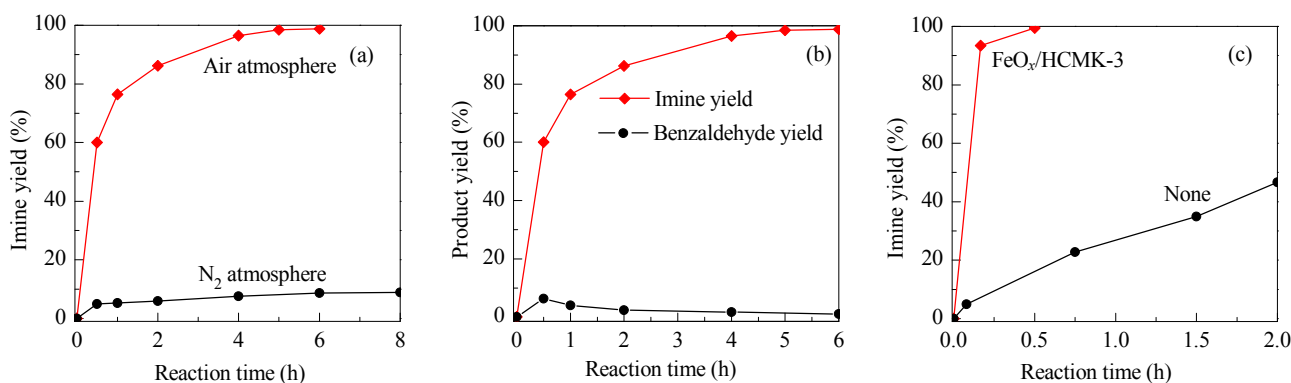


**Fig. 10.** (a) Effects of catalytic conditions on performance of FeO<sub>x</sub>/HCMK-3 in imine formation by aerobic oxidative coupling of benzyl alcohol and aniline. Reaction conditions: benzyl alcohol 1 mmol, aniline 2 mmol, catalyst 0.3 g, toluene 10 mL, 80 °C, air or N<sub>2</sub> 1 bar. (b) Time dependence of imine formation by oxidative coupling of benzyl alcohol and aniline over FeO<sub>x</sub>/HCMK-3. Reaction conditions: benzyl alcohol 1 mmol, aniline 2 mmol, catalyst 0.3 g, toluene 10 mL, 80 °C, air 1 bar. (c) Time dependences of imine formation by coupling of benzaldehyde and aniline with and without FeO<sub>x</sub>/HCMK-3 catalyst. Reaction conditions: benzaldehyde 1 mmol, aniline 2 mmol, catalyst 0.3 g, toluene 10 mL, 80 °C, air 1 bar.

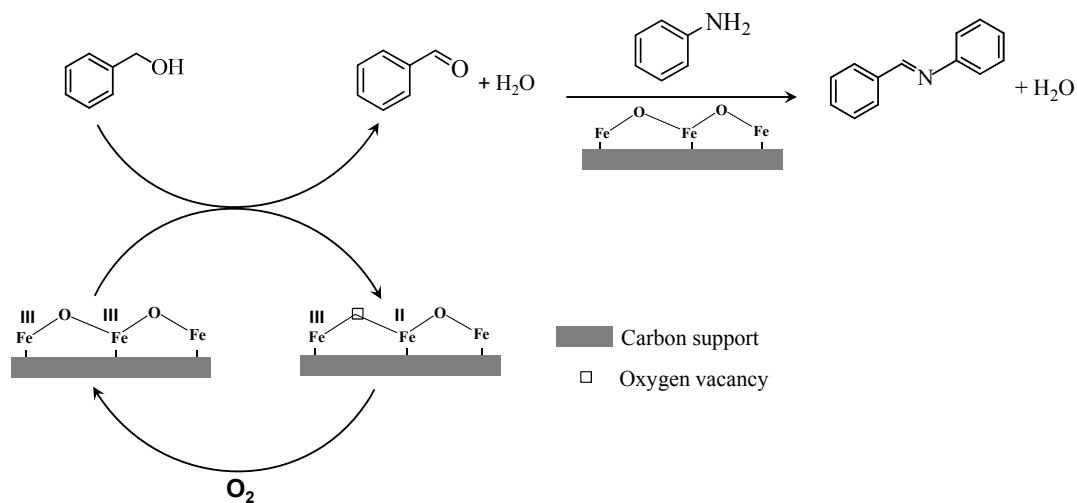
hyde might be an intermediate and that the reaction proceeds in two consecutive steps: (1) oxidative dehydrogenation of the alcohol to benzaldehyde and (2) imine formation by reaction of benzaldehyde with aniline.

We recently reported that FeO<sub>x</sub>/HCMK-3 catalyzes the oxidation of benzyl alcohol to benzaldehyde with air as the oxygen source [33]. Benzyl alcohol conversion of 72% was observed after reaction for 8 h. In the imine synthesis, benzyl alcohol conversion improved to 98.8% after reaction for 6 h. The second step in imine formation accelerates the conversion of benzyl alcohol. Fig. 10c shows that FeO<sub>x</sub>/HCMK-3 efficiently catalyzes imine synthesis from benzaldehyde and aniline. The reaction rate is 372.8 mmol h<sup>-1</sup> g<sup>-1</sup> (calculated based on iron oxide sites), which is 4.5 times higher than that for imine formation from benzyl alcohol and aniline (82.0 mmol h<sup>-1</sup> g<sup>-1</sup>). This confirms that oxidative dehydrogenation of alcohol is the rate-determining step in the reaction. Based on the above results and related literature reports [49,50], a plausible reaction mechanism for imine formation from an alcohol and aniline on FeO<sub>x</sub>/HCMK-3 is proposed (Scheme 1). Oxidative dehydrogena-

tion of benzyl alcohol by oxygen species occurs at the redox sites of FeO<sub>x</sub>/HCMK-3. Iron is reduced from valence +3 to +2. The produced benzaldehyde reacts with aniline over FeO<sub>x</sub>/HCMK-3 to afford the corresponding imine. FeO<sub>x</sub>/HCMK-3 is regenerated by oxidation of the reduced FeO<sub>x</sub>/HCMK-3 with O<sub>2</sub>.

#### 4. Conclusions

FeO<sub>x</sub>/HCMK-3 with highly dispersed iron oxide species shows high activity and recyclability in aerobic oxidative coupling of alcohols and amines to imines. The excellent catalytic performance of FeO<sub>x</sub>/HCMK-3 is ascribed to its high reducibility. The lattice oxygens in FeO<sub>x</sub>/HCMK-3 can participate in imine synthesis, and the reaction follows a redox mechanism over FeO<sub>x</sub>/HCMK-3. Two consecutive steps are involved in the reaction: oxidative dehydrogenation of an alcohol to an aldehyde and coupling of the aldehyde with an amine to an imine. Oxidative dehydrogenation of alcohol is the rate-determining step in the reaction.



**Scheme 1.** Proposed reaction mechanism for imine formation over FeO<sub>x</sub>/HCMK-3.

## References

- [1] Z. B. Han, Z. Wang, X. M. Zhang, K. L. Ding, *Angew. Chem. Int. Ed.*, **2009**, 48, 5345–5349.
- [2] A. J. A. Watson, J. M. J. Williams, *Science*, **2010**, 329, 635–636.
- [3] J. Gawronski, N. Wascinska, J. Gajewy, *Chem. Rev.*, **2008**, 108, 5227–5252.
- [4] S. I. Murahashi, *Angew. Chem. Int. Ed.*, **1995**, 34, 2443–2465.
- [5] J. F. Soulé, H. Miyamura, S. Kobayashi, *Asian J. Org. Chem.*, **2012**, 1, 319–321.
- [6] R. D. Patil, S. Adimurthy, *Asian J. Org. Chem.*, **2013**, 2, 726–744.
- [7] V. Kumar, S. Sharma, U. Sharma, B. Singh, N. Kumar, *Green Chem.*, **2012**, 14, 3410–3414.
- [8] L. Ravishankar, S. A. Patwe, N. Gosarani, A. Roy, *Synth. Commun.*, **2010**, 40, 3177–3180.
- [9] J. S. M. Samec, A. H. Éll, J. E. Bäckvall, *Chem. Eur. J.*, **2001**, 11, 2327–2334.
- [10] B. Chen, L. Y. Wang, S. Gao, *ACS Catal.*, **2015**, 5, 5851–5876.
- [11] Q. Kang, Y. G. Zhang, *Green Chem.*, **2012**, 14, 1016–1019.
- [12] S. Sithambaram, R. Kumar, Y. C. Son, S. L. Suib, *J. Catal.*, **2008**, 253, 269–277.
- [13] R. Cano, D. J. Ramón, M. Yus, *J. Org. Chem.*, **2011**, 76, 5547–5557.
- [14] Z. X. Zhang, Y. H. Wang, M. Wang, J. M. Lü, L. H. Li, Z. Zhang, M. R. Li, J. Y. Jiang, F. Wang, *Chin. J. Catal.*, **2015**, 36, 1623–1630.
- [15] H. W. Tian, X. C. Yu, Q. Li, J. X. Wang, Q. Xu, *Adv. Synth. Catal.*, **2012**, 354, 2671–2677.
- [16] B. Gnanaprakasam, J. Zhang, D. Milstein, *Angew. Chem.*, **2010**, 122, 1510–1513.
- [17] J. F. Soulé, H. Miyamura, S. Kobayashi, *J. Am. Chem. Soc.*, **2011**, 133, 18550–18553.
- [18] L. Tang, H. Y. Sun, Y. F. Li, Z. G. Zha, Z. Y. Wang, *Green Chem.*, **2012**, 14, 3423–3428.
- [19] H. Sun, F. Z. Su, J. Ni, Y. Cao, H. Y. He, K. N. Fan, *Angew. Chem. Int. Ed.*, **2009**, 48, 4390–4393.
- [20] W. He, L. D. Wang, C. Y. Sun, K. K. Wu, S. B. He, J. P. Chen, P. Wu, Z. K. Yu, *Chem. Eur. J.*, **2011**, 17, 13308–13317.
- [21] D. Gnanamgari, E. L. O. Sauer, N. D. Schley, C. Butler, C. D. Incarvito, R. H. Crabtree, *Organometallics*, **2009**, 28, 321–325.
- [22] A. Corma, T. Ródenas, M. J. Sabater, *Chem. Eur. J.*, **2010**, 16, 254–260.
- [23] S. Kegnaes, J. Mielby, U. V. Mentzel, C. H. Christensen, A. Riisager, *Green Chem.*, **2010**, 12, 1437–1441.
- [24] L. L. Zhang, W. T. Wang, A. Q. Wang, Y. T. Cui, X. F. Yang, Y. Q. Huang, X. Y. Liu, W. G. Liu, J. Y. Son, H. Oji, T. Zhang, *Green Chem.*, **2013**, 15, 2680–2684.
- [25] M. Tamura, K. Tomishige, *Angew. Chem. Int. Ed.*, **2015**, 54, 864–867.
- [26] B. Chen, J. Li, W. Dai, L. Y. Wang, S. Gao, *Green Chem.*, **2014**, 16, 3328–3334.
- [27] L. Y. Wang, B. Chen, L. H. Ren, H. Y. Zhang, Y. Lü, S. Gao, *Chin. J. Catal.*, **2015**, 36, 19–23.
- [28] A. H. Lu, J. J. Nitz, M. Comotti, C. Weidenthaler, K. Schlichte, C. W. Lehmann, O. Terasaki, F. Schüth, *J. Am. Chem. Soc.*, **2010**, 132, 14152–14162.
- [29] H. M. Torres Galvis, J. H. Bitter, C. B. Khare, M. Ruitenbeek, A. I. Dugulan, K. P. de Jong, *Science*, **2012**, 355, 835–838.
- [30] Z. X. Wu, W. Li, P. A. Webley, D. Y. Zhao, *Adv. Mater.*, **2012**, 24, 485–491.
- [31] A. R. Rajenahally, A. E. Surkus, H. Junge, M. M. Pohl, J. Radnik, J. Rabeah, H. Huan, V. Schünemann, A. Brückner, M. Beller, *Science*, **2013**, 342, 1073–1076.
- [32] S. A. Cotton, *Annu. Rep. Prog. Chem., Sect. A*, **2005**, 101, 208–230.
- [33] L. L. Geng, X. Y. Zhang, W. X. Zhang, M. J. Jia, G. Liu, *Chem. Commun.*, **2014**, 50, 2965–2967.
- [34] L. L. Geng, M. Zhang, W. X. Zhang, M. J. Jia, W. F. Yan, G. Liu, *Catal. Sci. Technol.*, **2015**, 5, 3097–3102.
- [35] D. Y. Zhao, J. L. Feng, Q. S. Huo, N. Melosh, G. H. Fredrickson, B. F. Chmelka, G. D. Stucky, *Science*, **1998**, 279, 548–552.
- [36] S. Jun, S. H. Joo, R. Ryoo, M. Kruk, M. Jaroniec, Z. Liu, T. Ohsuna, O. Terasaki, *J. Am. Chem. Soc.*, **2000**, 122, 10712–10713.
- [37] G. Liu, Y. Liu, Z. L. Wang, X. Z. Liao, S. J. Wu, W. X. Zhang, M. J. Jia, *Microporous Mesoporous Mater.*, **2008**, 116, 439–444.
- [38] L. L. Geng, S. J. Wu, Y. C. Zou, M. J. Jia, W. X. Zhang, W. F. Yan, G. Liu, *J. Colloid Interface Sci.*, **2014**, 421, 71–77.
- [39] M. Zhang, W. C. Zhu, G. Liu, X. Y. Zhang, Y. H. Zu, W. X. Zhang, W. F. Yan, M. J. Jia, *Chin. J. Catal.*, **2012**, 33, 465–472.
- [40] X. Zhang, Y. A. Niu, X. D. Meng, Y. Li, J. D. Zhao, *CrystEngComm*, **2013**, 15, 8166–8172.
- [41] J. L. Tu, M. Y. Ding, Q. Zhang, Y. L. Zhang, C. G. Wang, T. J. Wang, L. L. Ma, X. J. Li, *ChemCatChem*, **2015**, 7, 2323–2327.
- [42] J. Yang, H. W. Zhang, M. H. Yu, I. Emmanuelawati, J. Zou, Z. G. Yuan, C. Z. Yu, *Adv. Funct. Mater.*, **2014**, 24, 1354–1363.
- [43] M. Monti, B. Santos, A. Mascaraque, O. R. Figuera, M. A. Niño, T. O. Menteş, A. Locatelli, K. F. McCarty, J. F. Marco, J. de la Figuera, *J. Phys. Chem. C*, **2012**, 116, 11539–11547.
- [44] M. D. Sánchez, P. Chen, T. Reinecke, M. Muhler, W. Xia,

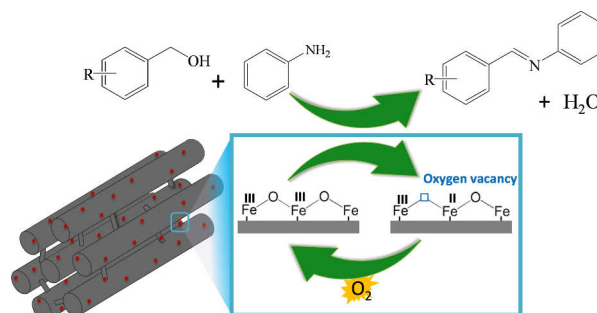
## Graphical Abstract

*Chin. J. Catal.*, 2016, 37: 1451–1460 doi: 10.1016/S1872-2067(16)62506-8

### Aerobic oxidative coupling of alcohols and amines to imines over iron catalysts supported on mesoporous carbon

Longlong Geng, Jinling Song, Bin Zheng, Shujie Wu, Wenxiang Zhang, Mingjun Jia, Gang Liu\*  
Jilin University

Mesoporous-carbon-supported iron oxide is a highly efficient and recyclable catalyst for imine synthesis by oxidative coupling of alcohols and amines with air as the oxygen source.



*ChemCatChem*, **2012**, 4, 1997–2004.

- [45] Q. Q. Zhuo, J. Gao, M. F. Peng, L. D. Bai, J. J. Deng, Y. J. Xia, Y. Y. Ma, J. Zhong, X. H. Sun, *Carbon*, **2013**, 52, 559–564.
- [46] X. L. Mou, B. S. Zhang, Y. Li, L. D. Yao, X. J. Wei, D. S. Su, W. J. Shen, *Angew. Chem. Int. Ed.*, **2012**, 51, 2989–2993.
- [47] L. Li, A. Q. Wang, B. T. Qiao, J. Lin, Y. Q. Huang, X. D. Wang, T. Zhang, *J. Catal.*, **2013**, 299, 90–100.
- [48] E. Zhang, H. W. Tian, S. D. Xu, X. C. Yu, Q. D. Xu, *Org. Lett.*, **2013**, 15, 2704–2707.
- [49] P. N. Amaniampong, Q. T. Trinh, B. Wang, A. Borgna, Y. Yang, S. H. Mushrif, *Angew. Chem. Int. Ed.*, **2015**, 54, 8928–8933.
- [50] U. Menon, V. V. Galvita, G. B. Marin, *J. Catal.*, **2011**, 283, 1–9.